Journal of Solid State Electrochemistry (2022) 26:2171–2182
https://doi.org/10.1007/s10008-022-05220-z

ORIGINAL PAPER

Novel lanthanum sulfide–decorated zirconia nanohybrid for enhanced electrochemical oxygen evolution reaction

F. F. Alharbi[1] · Mehar Un Nisa[2] · Hassan Mohamed Ahmed Hassan[3] · Sumaira Manzoor[2] · Zahoor Ahmad[4] · Abdul Ghafoor Abid[2] · Salma Aman[5] · Muhammad Naeem Ashiq[2] · Karam S. El-Nasser[6,7] · Taha Abdel Mohaymen Taha[8,9]

Received: 6 April 2022 / Revised: 31 May 2022 / Accepted: 8 June 2022 / Published online: 24 June 2022

Abstract

Metal sulfide and oxides have drawn interest as economical substitutes to noble metal catalysts due to their ability for oxygen evolution reaction (OER) activities. The inability of many sulfides and oxide nanocomposite materials has been produced in recent years to significantly boost their low OER activity. In the current study, we fabricated a novel lanthanum sulfide (La_2S_3) nanocrystal decorated on zirconium dioxide (ZrO_2) nanoflakes for OER electrocatalyst. The composite attains a low overpotential of 280 mV at a current density of 10 mA/cm^2 and outstanding stability of 30 h. The increased catalytic activity of the Zr-O–O superoxo group is responsible for the transfer of electron tendency from La species to ZrO_2, which favors the rupture of the bond of Zr–O in the steady arrangement. Hence, the present work developed an efficient La_2S_3-decorated ZrO_2-based oxygen evolution electrocatalyst instead of using rare earth viable catalysts like ruthenium oxide (RuO_2) or iridium oxide (IrO_2).

Keywords Water splitting · Nanohybrid · La_2S_3/ZrO_2 · OER · Alkaline media

✉ Muhammad Naeem Ashiq
naeembzu@bzu.edu.pk

[1] Department of Physics, College of Science, Princess Nourah bint Abdulrahman University (PNU), P.O. Box 84428, Riyadh 11671, Saudi Arabia

[2] Institute of Chemical Sciences, Bahauddin Zakariya University, Multan 60800, Pakistan

[3] Department of Chemistry, College of Science, Jouf University, Sakaka 2014, Saudi Arabia

[4] Department of Chemistry, University of Engineering and Technology (UET), Lahore, Pakistan

[5] Department of Physics, Khwaja Fareed University of Engineering and Information Technology, Abu Dhabi Road, Rahim Yar Khan, Pakistan

[6] Chemistry Department, College of Science and Arts, Jouf University, P.O. Box 756, Al-Gurayyat, Saudi Arabia

[7] Chemistry Department, Faculty of Science, Al-Azhar University, Assiut 71524, Egypt

[8] Physics Department, College of Science, Jouf University, P.O. Box 2014, Sakaka, Saudi Arabia

[9] Physics and Engineering Mathematics Department, Faculty of Electronic Engineering, Menoufia University, Menouf 32952, Egypt

Introduction

Scientists have been working hard to invent efficient, low-cost, ecologically acceptable alternative energy conversion and storage methods to fulfill rising energy demands as well as those have no hazardous effect on the environment [1–6]. Electrolysis cells [7], fuel cells [8], and metal-air batteries [9] are only a few of the ways in which the chemical energy is turned into electrical energy. These devices go through steps with sluggish multi-electron transfer mechanism of both oxygen evolution reaction (OER) and hydrogen evolution reaction (HER) [10–13]. Engineering economical, high-efficiency electrocatalysts for OER are crucial for renewable energy systems [14]. Precious metal catalysts with high catalytic performance include Pd and few other precious metals, like Ag, Au, Ru, Ir, and Pt. Furthermore, Gokhan et al. synthesized the Ag/AgO-based nanocomposite employed toward water splitting process. The electrochemical result revealed that Ag/AgO nanoparticle exhibited 600 mV overpotential at 1 mA/cm^2 current density and lower Tafel slope of 80 mV/dec [15]. Yeo and Bell developed the cobalt oxide decorated on surface of Au nanoparticles employed toward electrocatalytic water splitting [16].

However, the electrocatalytic water splitting results of Ru, Ir, and pt display the Tafel slope of 44, 64, and 143 mV and onset potential of 1.54, 1.56, and 1.86 potential at 0.5 mA/mol 10^9/V, respectively, and suggest that noble metals are potential candidate for oxygen evolution reaction [17–19]. Due to their high cost and rarity, their commercial uses are limited [20]. On the other hand, the performance of an OER electrocatalyst is greatly influenced by pH of the electrolytes. An alkaline solution, rather than a neutral or acidic solution, is best for OER electrocatalysis. In recent studies, different transition metals show variable behavior in different electrolyte medium. However, noble metals such Pt, Ir and Ru shows great OER activity in alkaline as well as acidic medium [21]. Furthermore, She et al. studied the Ir-based electrocatalyst under the acidic medium for the oxygen evolution reaction process which exhibited an overpotential of 0.37 V [22]. Xu et al. synthesized IrRu@Te and employed toward OER activity in the acidic medium (0.5 M H_2SO_4). The electrochemical result revealed that fabricated electrode display stability for 20 h and 50 mV overpotential at 10 mA/cm^2 current density [23]. However, Zhang et al. synthesized a Ru-based NiMo electrocatalyst and studied their electrochemical performance by employing toward OER activity result display the lower tafel slope value of 110 mV/dec and 280 mV overpotential at the current density of 10 mA/cm^2 under 1 M KOH [24]. So in most of the cases, the OER efficiency was excellent in alkaline media therefore in the present work alkaline media has been chosen.

Various non-noble electrode materials have been studied in the OER process as prospective of noble metal electrodes replacements. Due to their electrocatalytic activity and non-noble metallic character, metal-free carbon compounds [25, 26], metallic alloys [27], metal oxides [28], metallic phosphides (MP) [29], metallic selenides (MS) [30], and carbon nitrides (CN) [31] have all been widely searched for OER [32]. The electrocatalysts due to their unique properties of an incompletely filled d-shell and increased electrical and thermal conductivity [33–35]. Non-precious metal-based compounds have been searched to avoid the usage of precious electrocatalysts in OER [36, 37] to reduce the sluggish OER kinetics [11]. A standard metric for determining this type of functionality (catalyst efficiency) is the potential difference (E) measured against the reversible hydrogen electrode (RHE) [38].

The transition metal sulfides, including Co [39], Cu [32, 40], Ni [41], and La [42], showed better efficiency as an OER catalysts which have been discovered in the last decade [43]. When compared to other precious catalysts like, Ru/C (1.01 V) [44] and Ir/C (0.85 V) [45], many researchers such as Liu et al. reported that IrO_2/ZrO_2 having tafel slope of 15 mV/dec [46]. Li et al. reported $Ni(OH)_2/ZrO_2$ tafel slope of 57 mV/dec in alkaline media [47]. To achieve a potential value of 263 mV, Mane et al. employed a one pot solvothermal approach to synthesize La_2S_3-MnS [42]. However, According to our findings, the catalytic activity of lanthanum sulfide substance in OER has been significantly improved than the previously estimated combined effect of OER. As a result, a high-performance lanthanum sulfide catalyst for OER has been developed.

Lanthanum sulfide must have active lanthanum sites to be used as an electrocatalyst. According to a prior study, the microchemical environment around the inner transition metal sites are preferable on metal-based catalysts [48]. Doping ions, supports, or other functional compositions can boost the activity of lanthanum centers [49, 50]. The synergetic effects of chemical coupling can lead to improved catalytic activity in composite catalysts as the OER performance of this catalyst is poor when performed as individual catalysts [51]. But single lanthanum sulphide has not good stability, and therefore, its composite with zirconia has been investigated. The titanium oxide has been widely used for various applications, and the zirconia is an isoelectronic with titania, and therefore, zirconia has been chosen as other material.

From the above motivated concern, herein, a highly active and stable OER electrocatalyst (La_2S_3 nanocrystals decorated on ZrO_2 nanoflakes) has been developed via hydrothermal technique. Precious metal-based catalysts in an alkaline electrolyte performance have been comparable with materials synthesized in the present work regarding OER activity. The Zr-O bond is anticipated to be broken in the stable state due to electron transfer between La and ZrO_2 (Zr-O-O superoxo group), enhancing the electrocatalytic performance. Hence, due to its outstanding OER performance, La_2S_3/ZrO_2 nanocomposite is a novel and potentially nonprecious oxygen evolution catalyst which can be used in future applications.

Experimental technique

Materials and methods

The zirconium dichloride oxide ($ZrOCl_2$), sodium sulfide nanohydrate ($Na_2S.9H_2O$) VETEC (98%), lanthanum nitrate hexahydrate ($La(NO_3)_3.6H_2O$), potassium hydroxide (KOH), citric acid, ($C_6H_8O_7$), Duksan hydrochloric acid (HCl) Merck (37%), ethanol (C_2H_5OH), Analar (99%), acetone (CH_3COCH_3) Normapur (99.8%), nitric acid (HNO_3), and ultrapure water.

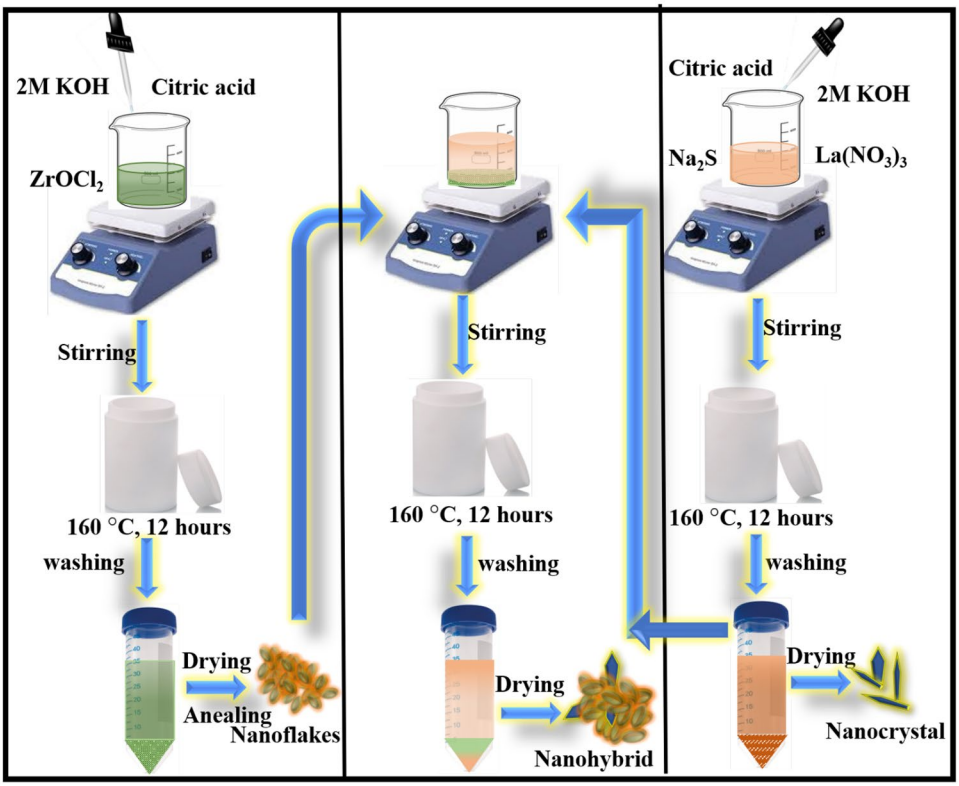

Scheme 1 Schematic illustration for the synthesis of all required products

Synthesis of ZrO_2

A zirconium dioxide nanoflake was synthesized using a hydrothermal technique. The 0.05 M zirconyl chloride and 2.0 M KOH solutions were prepared in deionized (DI) water separately, and 0.1 mM solution of citric acid was also added to the zirconyl chloride solution. The solution of KOH was then added drop-by-drop in the solution mentioned above. The entire solution was transferred into a 100 mL Teflon-lined (T.L) autoclave and placed for 12 h at 160 °C in an oven. At room temperature, the autoclave was allowed to cool after 12 h. Subsequently, the obtained precipitates were centrifuged and washed many times with DI water and ethanol which were finally dried overnight at 80 °C. After that, the resultant precipitate was ground and annealed for 3 h at 450 °C in the furnace. The powder was collected and kept for further procedure.

Synthesis of La_2S_3/ZrO_2

Nanohybrid La_2S_3/ZrO_2 was synthesized using the hydrothermal technique. In this case, 0.05 M solution of lanthanum nitrate was prepared in deionized water, and 0.1 mM citric acid was also mixed under stirring. The weighed amount of already fabricated ZrO_2 (equivalent to 0.05 M) was also mixed and stirred for a further 3 h to homogenize it. After that, sodium sulfide (0.05 M) was added to the above mixture and placed on the magnetic hotplate with continuous stirring. After 3 h of constant stirring, solution was transferred to a T.L autoclave and kept in an electric oven at 160 °C for 12 h. The autoclave was cooled to room temperature, and the obtained precipitates were centrifuged and washed many times with DI water, ethanol, and dried overnight at 80 °C. A similar method was used to synthesize La_2S_3 for comparison purposes except the addition of ZrO_2 (Scheme 1).

Physical characterizations and electrode preparation

X-ray diffraction (XRD), scanning electron microscopy (SEM), Brunauer–Emmett–Teller (BET), and x-ray photoelectron spectroscopy (XPS) analyses was used for the characterization of fabricated materials to confirm the structural, morphological, and surface properties. A Bruker D8 Advance Powder X-ray diffractometer was used to conduct XRD experiments on monochromatized CuKα (0.15407 nm). The BET surface area, pore size, and pore volume were confirmed using NOVA-2200 E. On the other hand, the drop cast technique was utilized to make La_2S_3, ZrO_2, and La_2S_3/ZrO_2 thin films of constant thicknesses (0.001 mm) on stainless steel substrate and was used as a working electrode. Before being employed as substrates, the stainless-steel plates (1×2 cm^2) were etched with oxalic acid, washed, and rinsed with deionized water. Electrochemical performances like linear sweep voltammetry (LSV), cyclic voltammetry

(CV), electrochemical impedance spectroscopy (EIS), and chronoamperometry were performed to examine the electrocatalytic activity of La2S3/ZrO2 nanocomposite in 1.0 M KOH aqueous electrolyte.

Electrochemical characterizations

AUTOLAB (PGSTAT-204) electrochemical workstation was used to manage the electrochemical investigation of fabricated materials using three-electrode setup. This experiment contains a catalyst-coated stainless-steel electrode, a Pt wire, and Ag/silver chloride as working, counter, and reference electrodes (saturated with 3.0 M KCl), respectively. Standard reversible hydrogen electrode (RHE) potential is calculated from the Ag/AgCl potential using the formula (1) for all viable measurements [52].

$$E_{\text{vs RHE}} = E_{vs\ \text{Ag/AgCl}} + E^{0}{}_{\text{Ag/AgCl}} + 0.059\ \text{pH} \quad (1)$$

The expression (2) was used to obtain the overpotential value:

$$\eta = E_{\text{vs RHE}} - 1.23\ \text{V} \quad (2)$$

The turnover frequency is another parameter to consider the material's catalytic effectiveness in an oxygen evolution reaction. It exhibits the ability of a catalyst to convert a substrate into a product in a unit of time under specific conditions. The following equation was used to calculate the turn over frequency of synthetic material.

$$\text{TOF} = I \times A/4 \times F \times m \quad (3)$$

Here, I indicate the current at a specific overpotential, A is the geometrical surface area, F represents the Faraday's constant, and m is the number of moles of active catalyst.

In the presence of Ag/AgCl, the LSV was performed at a different scan rate in 1.0 M KOH with the voltage fluctuating between 0.02 and 0.07 V/s. As a result, the oxygen evolution currents start to change slightly. The electrochemical measurement were performed in 1.0 M alkaline electrolyte (KOH) with a potential range of 1.00 to –1.00 V (against Ag AgCl). A stability test was carried out using chronoamperometric recorded at 0.75 V applied potential. Electrochemical impedance spectroscopy (EIS) was done at open circuit potentials with frequencies ranging from 100 kHz to 10 MHz. The amplitude employed in EIS testing was set at 5 mV, taking the potential applied of 0.50 V.

Results and discussion

Structural analysis

The structure and phase orientation of all the fabricated samples were analyzed using powder X-ray diffraction (PXRD). The powder X-ray diffraction pattern of synthesized La_2S_3, ZrO_2, and La_2S_3/ZrO_2 with their standard JCPDS pattern in the range of $2\theta = 20–80°$ is shown in Fig. 1. The diffraction peaks of La_2S_3 demonstrated at $2\theta = 20.8°$, 24.2°, 28.5°, 29.5°, 31.2°, 34.6°, 35.1°, 38.3°, 39.9°, 41.2°, 43.5°, 44.2°, 49.4°, 50.3°, 54.1°, 55.7°, 57.3°, 60.5°, 62.7°, 65.3°, 71.2°, 75.9°, and 77.0° are well-matched with JCPDS No. 00–022-0645 indicating that there is no impurity phase. The diffraction peaks of the ZrO_2 were indexed at $2\theta = 24.5°$, 27.3°, 31.4°, 34.3°, 35.2°, 38.2°, 40.7°, 45.3°, 48.9°, 50.3°, 54.1°, 55.4°, 57.6°, 59.1°, 61.5°, 62.3°, 65.6°, 69.1°, 71.0°, 72.8°, 74.6°, and 78.1° (JCPDS No. 00–001-0750) belonging to space group P2/c and space group number 13. The sharp peaks define the crystalline nature of the prepared La_2S_3, ZrO_2, and La_2S_3/ZrO_2. There is no undesirable diffraction peak appeared in the nanocomposite, endorsing the purity and successful synthesis of the composite. Hence, the nanohybrid La_2S_3/ZrO_2 contains all the peaks of its counterparts with a slight change in its peak position and intensity.

Morphological analysis

The morphology and size of the material played a significant role in the variation of electrochemical parameters. Scanning electron microscopy studied the La_2S_3/ZrO_2 nanohybrid and its counterparts, i.e., La_2S_3, ZrO_2 materials synthesized by hydrothermal route as shown in Fig. 2a–d. The obtained ZrO_2 and La_2S_3 are infused nanoflakes and nanocrystals shape, respectively (Fig. 2a, b). The growth of the nanocrystals of La_2S_3 on the ZrO_2 fused nanoflakes forming nanohybrid as displayed in Fig. 2c, d. The surface of the ZrO_2 is packed with La_2S_3 particles ranging in size from 250 to 400 nm, and they appear to be distributed throughout the material. The ZrO_2 is filled with irregular La_2S_3 nanocrystals, as shown in micrographs (Fig. 2c, d). Hence, the modified morphology of La_2S_3/ZrO_2 plays a significant role in nanohybrid formation as well as in electrochemical properties. The EDX spectrum of La_2S_3/ZrO_2 are shown in Fig. 2e. Only lanthanum, sulphur, zirconium, and oxygen elements were found, and no other element was found, proving the synthesized La_2S_3/ZrO_2 material.

XPS analysis

XPS spectra examined the synthesized material. Using Gaussian fitting, the deconvoluted peaks were obtained for deep study. According to the survey spectrum of La_2S_3/ZrO_2 comprising only La, S, Zr, C, and O, as displayed in Fig. 3a, there is no other element except the investigated material which was also confirmed by the EDX analysis. Using the curve fitting approach, three Gaussian peaks were detected for the O 1 s core level, as shown in Fig. 3b. Metal–oxygen is visible in the first peak at 530.2 eV, and

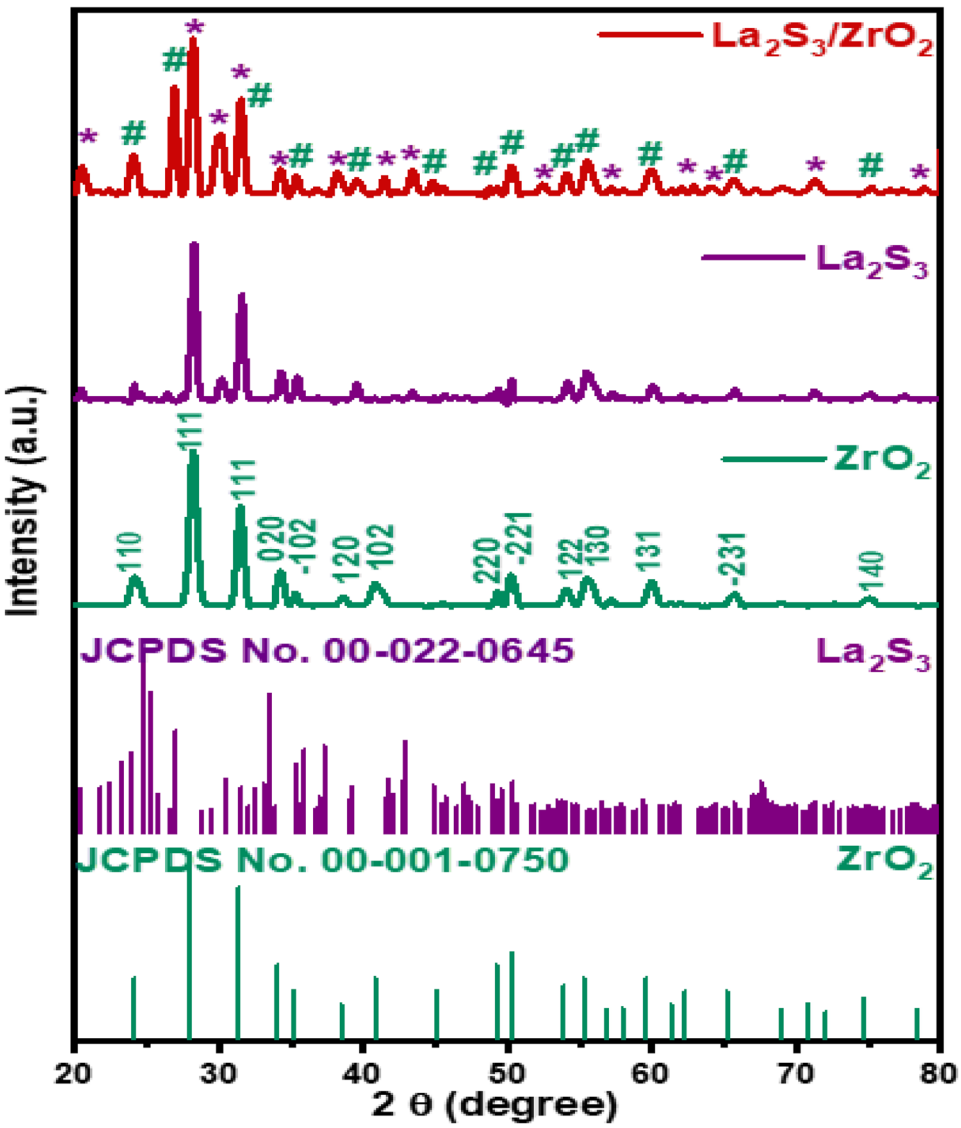

Fig. 1 XRD pattern of ZrO_2, La_2S_3 with their respective standard reference patterns and La_2S_3/ZrO_2

the last peak which was found at 532.5 eV corresponds to O_2. The 285 eV C 1 s peak seen in Fig. 3c is used for XPS peak correction. Peaks that can be found on the high beam-energy side of the La 3d are assigned to $3d_{5/2}$, and $3d_{3/2}$ for the peaks at 834.2 and 851.2 eV, correspondingly resulting in +3 oxidation state (Fig. 3d). In the high-resolution S 2p spectrum, an exceedingly faint doublet at 163.3 eV corresponds to S 2p1/2, as shown in Fig. 3e, and the presence of oxygen sulfur (O-S) connection in the molecule is confirmed by the peak at 167.7 eV confirming the −2-valance state for sulphur. The fitted spectra of the Zr 3d spin–orbit doublet peaks are presented in Fig. 3f with a 2.1-eV energy separation having binding energy at 181.8 and 183.9 eV correlated to Zr $3d_{5/2}$ and Zr $3d_{3/2}$ contributions, correspondingly confirming the +4-valence state of Zr. This proved the successful formation of the La2S3/ZrO2 nanocomposite.

The Fig. 3g the material adsorption/desorption isotherm resultant from BET had mesoporous structures such as the H3 hysteresis loop. The consequent surface areas of ZrO_2, La_2S_3, and La_2S_3/ZrO_2 nanocomposite were 340 m^2/g, 455 m^2/g, and 612 m^2/g, respectively. The resultant pore volumes for the ZrO_2, La_2S_3, and La_2S_3/ZrO_2 were 0.91, 1.12, and 2.05 cm^3/g, respectively. Among all, the La_2S_3/ZrO_2 nanocomposite may have better electrocatalytic activity than either La_2S_3 and ZrO_2 due to its larger surface area, pore volume, porosity, and more active sites on the surface.

Electrochemical performance

The performance of La_2S_3, ZrO_2, and La_2S_3/ZrO_2 nanohybrid deposited on stainless steel strip (SSS) in 1.0 M KOH solution was investigated using LSV at a scan rate of 5 mV/s after electrochemical preconditioning with 20

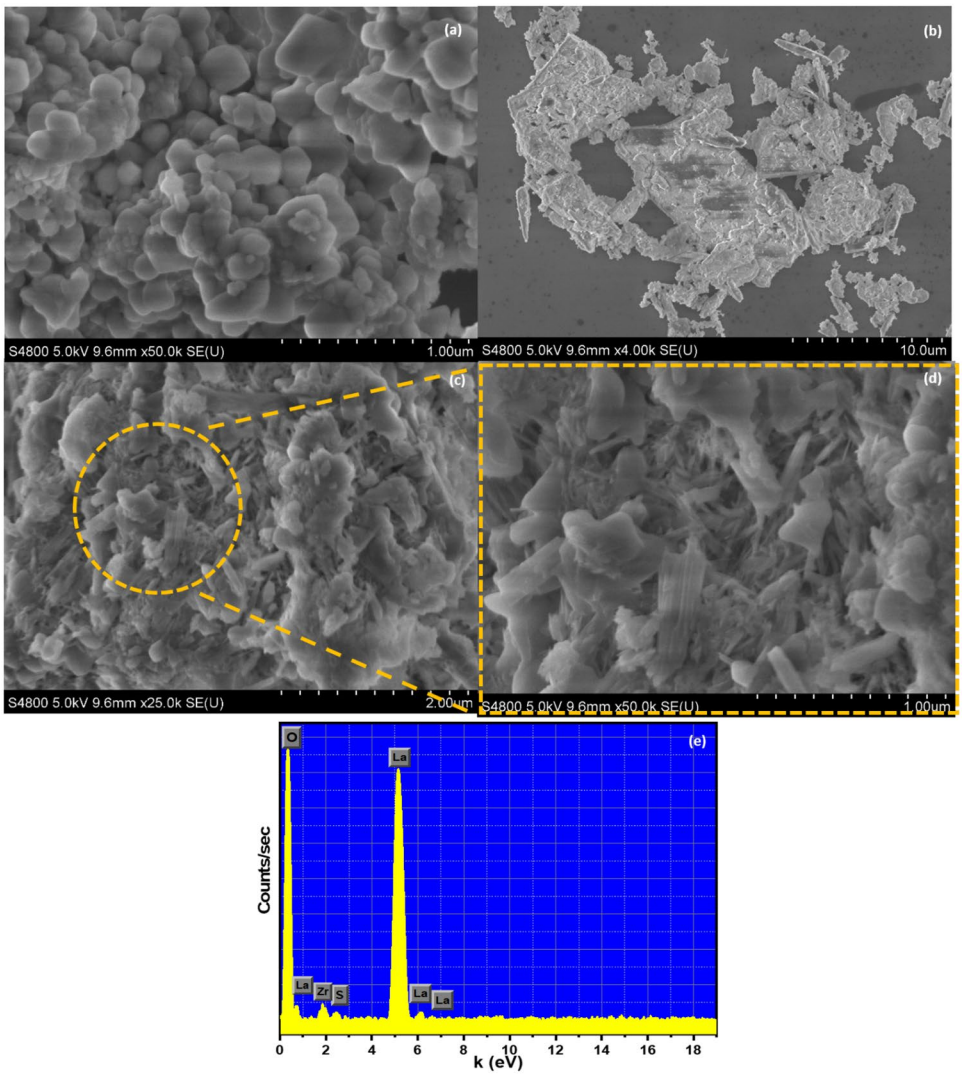

Fig. 2 SEM micrographs of **a** ZrO_2, **b** La_2S_3, **c** La_2S_3/ZrO_2 nanocomposite, **d** enlarged SEM micrograph, and **e** EDX of La_2S_3/ZrO_2

cyclic voltammetric scans using the three-electrode system. Figure 4a shows the linear sweep voltammogram of all the synthesized products and state of the art RuO_2 material deposited on the stainless-steel surface. Among all the fabricated materials, the nanocomposite behaves a remarkable response to achieve oxygen evolution content. The enhanced efficiency of the nanohybrid was due to the presence of transition metal ions that can be employed as donor–acceptor chemisorption sites, and also, high conductivity can be achieved by hopping between cations with different valence states. The La_2S_3/ZrO_2 nanocomposite showed the onset potential closest to the other rare metal and much lower than the La_2S_3 and ZrO_2. In the nanocomposite, the synergistic effect occurs considering ZrO_2 and La_2S_3, which is principally responsible for the significant OER activity.

The OER performance of the prepared samples was determined by another important parameter, such as overpotential at a current density of 10.0 mA/cm^2 using 1.0 M alkaline KOH solution. The resultant overpotentials of La_2S_3, ZrO_2, RuO_2, and La_2S_3/ZrO_2 nanocomposite were 390, 420, 320, and 280 mV, respectively, as shown in Fig. 4b. On the other hand, the overpotentials of the composite material at current densities of 50 and 100 mA/cm^2 were found to be 521 and 656 mV, respectively. The lower value of the overpotential for composite indicates better catalytic performance for OER because the single metal sulfides are less stable than transition metal oxide/hydroxide. Even though the La_2S_3/ZrO_2 still outperforms many other catalysts when tested with a stainless-steel electrode at a current density of 10.0 mA/cm^2 due to the presence of both sulfides and oxides, as given in Table 1. Hence, the resultant comparison analysis shows that La_2S_3/ZrO_2 product has remarkable catalytic activity.

Figure 4c shows the results for calculating the catalyst's intrinsic electrocatalytic activity using their turnover

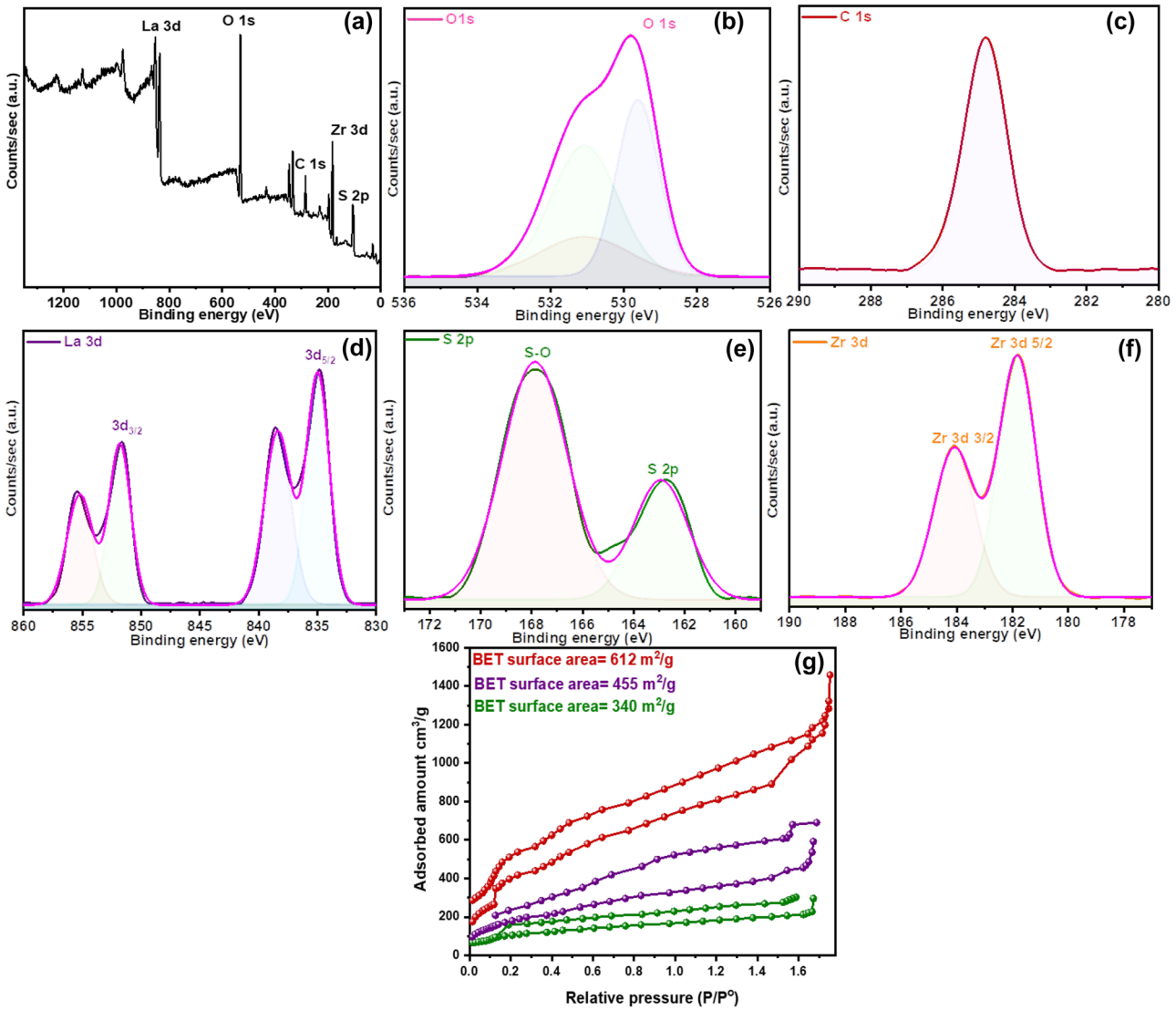

Fig. 3 **a** Survey spectrum of the nanohybrid; XPS spectrum for **b** C1s, **c** O1s, **d** S 3d, **e** La 3d, **f** Zr 3d, and **g** BET isotherm of La_2S_3/ZrO_2, La_2S_3, and ZrO_2

frequencies (TOFs). The TOF can be calculated via the Eq. (3) relation as [12]. The calculated TOF for ZrO_2, La_2S_3, and La_2S_3/ZrO_2 were 0.0006/s, 0.0019/s, and 0.0025/s, respectively. The results depict that La_2S_3/ZrO_2 has the highest TOF at 1.5 V, which is 0.105 times higher than ZrO_2 and 0.09 times that of La_2S_3. The greater the TOF, the higher will be the efficiency of the catalyst.

The Nyquist plots from the EIS measurements are examined under basic conditions using an equivalent circuit fitting, as shown in Fig. 4d. The charge transfer resistance (Rct) of ZrO_2, La_2S_3, and La_2S_3/ZrO_2 were 83.77 Ω, 81.49 Ω, and 40.12 Ω. When comparing the various Rct values, it is clear that the fabricated nanocomposite significantly improves charge transfer efficiency and, as a result, OER kinetics due to the synergistic effect between ZrO_2 and La_2S_3.

Electrochemical surface area (ECSA) can be determined using cyclic voltammetry in non-Faradaic regions and was calculated using the following relation [62]:

$$C_{\mathrm{dl}} = \mathrm{slope}/2 \tag{4}$$

$$\mathrm{ECSA} = C_{\mathrm{dl}}/C_s \tag{5}$$

Slope of the plot Δj vs. scan rate is divided by 2 for the calculation of C_{dl} and by considering the specific capacitance value ($C_s = 0.04$ μF/cm^2) as reported previously for all flat electrodes. The calculated ECSA for ZrO_2, La_2S_3,

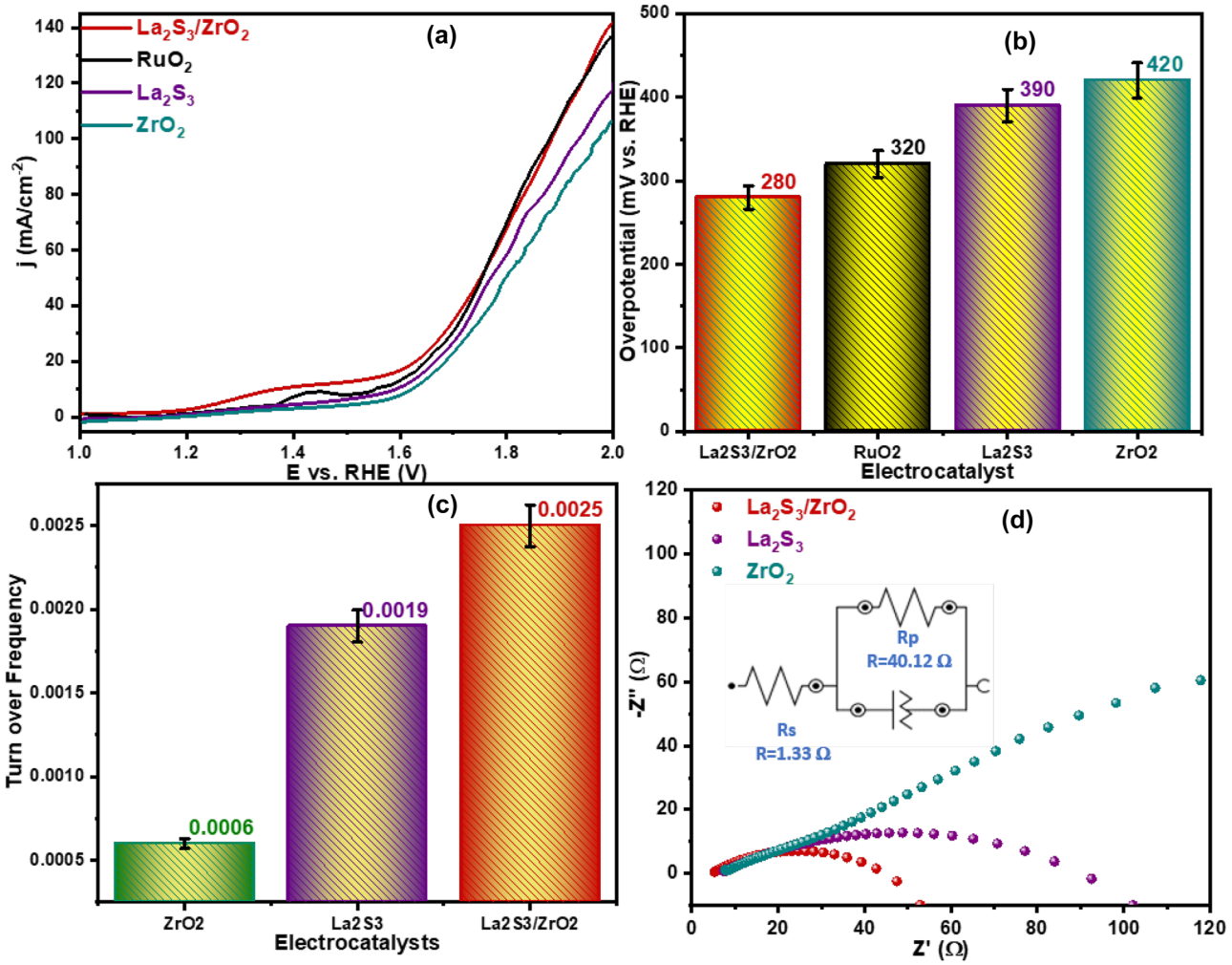

Fig. 4 **a** Linear sweep voltammogram, **b** overpotential comparison, **c** Turn over frequency, and **d** EIS for ZrO_2, La_2S_3, and La_2S_3/ZrO_2 (inset circuit diagram) in the alkaline environment for OER

and La_2S_3/ZrO_2 were 93.75 cm^2, 150 cm^2, and 170 cm^2, respectively. It was shown in Fig. 5 that La_2S_3/ZrO_2 nanocomposite has the highest C_{dl} (6.8 mF/cm^2) and ECSA (170 cm^2), which indicates that a higher ECSA allows for more electrochemical active sites and thus improves OER activity.

The long-term stability of catalytic electrodes is crucial in commercial applications. We investigated the OER stability of the La_2S_3/ZrO_2 composite in an alkaline electrolyte using the (i-t) curve via chronoamperometry. Figure 6 shows the *i-t* graph of the La_2S_3/ZrO_2 composite and responds a straight line with just a slight drop, confirming the high stability of the composite material for electrochemical water oxidation up to 30 h, as shown in Fig. 6a. To confirm the stability of the resultant material after long term of 30 h stability, XRD analysis was performed, showing that the phase structure remains same while a little bit intensity of the peaks was changed as shown in Fig. 6b. Hence, the La_2S_3/ZrO_2 nanocomposite performs the promising OER electrocatalyst because of its high OER activity and long-term stability.

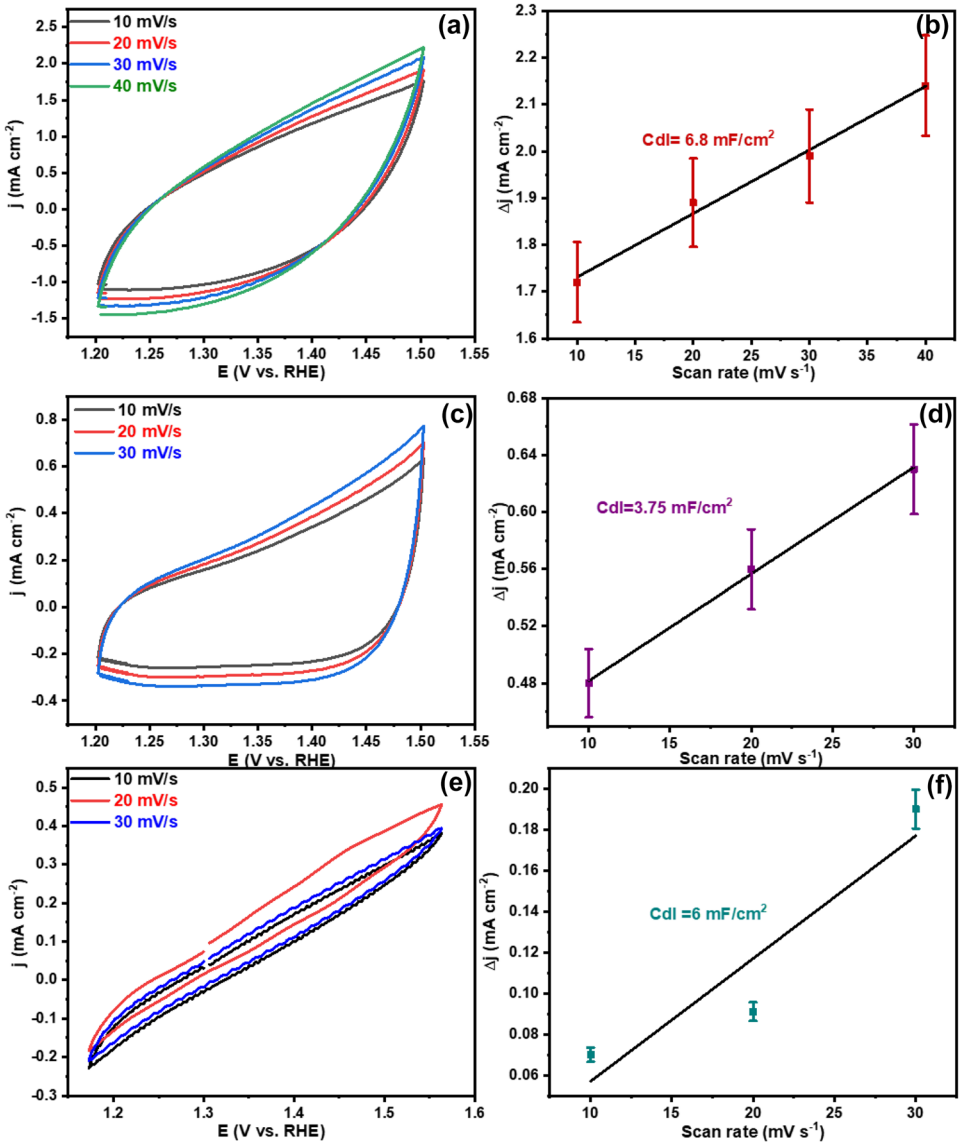

Fig. 5 **a**, **c**, **e** CV curves; **b**, **d**, **f** double-layer capacitance of La_2S_3/ZrO_2, ZrO_2, and La_2S_3

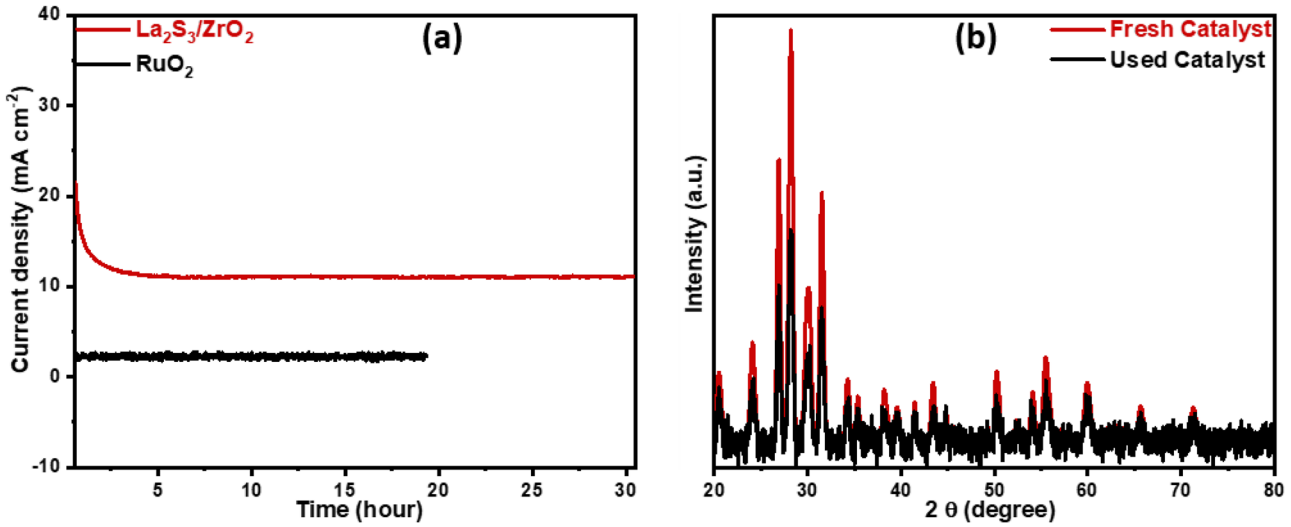

Fig. 6 **a** Chronoamperometry; **b** XRD pattern before and after electrochemical study of La_2S_3/ZrO_2

Table 1 Comparative study with the already reported oxide- and sulfide-based materials

Sr. no	Composition	Overpotential	Substrate	Reference
1	ZrP_2S_6@ $MoTe_2$	280 mV	Pencil graphite	[53]
2	$CeO_2/CoSe_2$ hybrid	288 mV	Glassy carbon	[54]
3	RuO_2/CeO_2	350 mV	Glassy carbon	[55]
4	Ni_3Se_2-Au	270 mV	Glassy carbon	[56]
5	$LaNi_{1-x}Fe_xO_3$	439 mV	Graphite sheet	[57]
6	Ru-NiFe-P	242 mV	Nickel Foam	[58]
7	W-NiCoP	330 mV	Nikel foam	[59]
8	La-doped CuO	320 mV	Stainless steel	[60]
9	Co-doped RuO	169 mV	Glass carbon	[61]
10	**La_2S_3/ZrO_2**	**280 mV**	**Stainless steel**	**This work**

Conclusion

In the present work, the La_2S_3/ZrO_2 nanohybrid was synthesized hydrothermally in an aqueous medium, and according to the SEM findings, the La_2S_3 nanocrystals decorated on ZrO_2 nanoflakes. At the same time, the X-ray photoelectron spectroscopy, EDX, and X-ray diffraction analyses revealed the elements oxidation states and the purity of the synthesized materials. The catalyst's electrochemical behavior was confirmed via LSV, EIS, and chronoamperometry, resulting in a lower overpotential of 280 mV compared to the individuals like La_2S_3 (390 mV) and ZrO2 (420 mV) because the nanocomposite has the most active sites due to higher surface area. The fabricated material also retained its stability after 30 h. It has the potential to be employed in electrochemical water splitting in the future due to its improved performance. As a result of this novel technique, chalcogenides open an advanced avenue for OER performance, which will better tuned, and allowing for improved water splitting and, more widely, increased applicability to electrochemical and optoelectronic property domains.

Acknowledgements The authors express their gratitude to Princess Nourah bint Abdulrahman University Researchers Supporting Project (Grant No. PNURSP2022R55), Princess Nourah bint Abdulrahman University, Riyadh, Saudi Arabia.

References

1. Abid AG, Manzoor S, Usman M, Munawar T, Nisa MU, Iqbal F, Ashiq MN, Najam-ul-Haq M, Shah A, Imran M (2021) Scalable synthesis of Sm_2O_3/Fe_2O_3 hierarchical oxygen vacancy-based gyroid-inspired morphology: with enhanced electrocatalytic activity for oxygen evolution performance. Energy Fuels 35:17820–17832
2. Rehman MY, Manzoor S, Nazar N, Abid AG, Qureshi AM, Chughtai AH, Joya KS, Shah A, Ashiq MN (2021) Facile synthesis of novel carbon dots@ metal organic framework composite for remarkable and highly sustained oxygen evolution reaction. J Alloys Compd 856:158038
3. Hao J, Yang W, Peng Z, Zhang C, Huang Z, Shi W (2017) A nitrogen doping method for CoS2 electrocatalysts with enhanced water oxidation performance. ACS Catal 7:4214–4220
4. Wang F, Xia L, Li X, Yang W, Zhao Y, Mao J (2021) Nano-ferric oxide embedded in graphene oxide: high-performance electrocatalyst for nitrogen reduction at ambient condition. Energy Environ Mater 4:88–94
5. Liu C, Zhou W, Zhang J, Chen Z, Liu S, Zhang Y, Yang J, Xu L, Hu W, Chen Y (2020) Air-assisted transient synthesis of metastable nickel oxide boosting alkaline fuel oxidation reaction. Adv Energy Mater 10:2001397
6. Chhetri K, Muthurasu A, Dahal B, Kim T, Mukhiya T, Chae S-H, Ko T, Choi Y, Kim H (2022) Engineering the abundant heterointerfaces of integrated bimetallic sulfide-coupled 2D MOF-derived mesoporous CoS2 nanoarray hybrids for electrocatalytic water splitting. Mater Today Nano 17:100146
7. Kim J, Jun A, Gwon O, Yoo S, Liu M, Shin J, Lim TH, Kim G (2018) Hybrid-solid oxide electrolysis cell: a new strategy for efficient hydrogen production. Nano Energy 44:121–126
8. Abdelkareem MA, Elsaid K, Wilberforce T, Kamil M, Sayed ET, Olabi A (2021) Environmental aspects of fuel cells: a review. Sci Total Environ 752:141803
9. Wang ZL, Xu D, Xu JJ, Zhang XB (2014) Oxygen electrocatalysts in metal–air batteries: from aqueous to nonaqueous electrolytes. Chem Soc Rev 43:7746–7786
10. Nisar L, Sadaqat M, Hassan A, Shah A, Najam-Ul-Haq M, Ashiq MN, Ehsan MF, Joya KS (2020) Ultrathin CoTe nanoflakes electrode demonstrating low overpotential for overall water splitting. Fuel 280:118666
11. Hassan A, Nisar L, Iqbal R, Sadaqat M, Hussain F, Ashiq MN, Najam-ul-Haq M, Shah A, Joya KS (2021) Copper telluride nanowires for high performance electrocatalytic water oxidation in alkaline media. J Power Sources 491:229628
12. Sadaqat M, Manzoor S, Nisar L, Hassan A, Tyagi D, Shah JH, Ashiq MN, Joya KS, Alshahrani T, Najam-ul-Haq M (2021) Iron doped nickel ditelluride hierarchical nanoflakes arrays directly grown on nickel foam as robust electrodes for oxygen evolution reaction. Electrochim Acta 371:137830
13. Liu PF, Yin H, Fu HQ, Zu MY, Yang HG, Zhao H (2020) Activation strategies of water-splitting electrocatalysts. J Mater Chem A 8:10096–10129
14. Nong HN, Falling LJ, Bergmann A, Klingenhof M, Tran HP, Spöri C, Mom R, Timoshenko J, Zichittella G, Knop-Gericke, (2020) A key role of chemistry versus bias in electrocatalytic oxygen evolution. Nature 587:408–413
15. Elmaci G (2020) Microwave assisted green synthesis of Ag/AgO nanocatalyst as an efficient OER catalyst in neutral media. Hittite J Sci Eng 7:61–65
16. Yeo BS, Bell AT (2011) Enhanced activity of gold-supported cobalt oxide for the electrochemical evolution of oxygen. J Am Chem Soc 133:5587–5593
17. Reier T, Oezaslan M, Strasser P (2012) Electrocatalytic oxygen evolution reaction (OER) on Ru, Ir, and pt catalysts: a comparative study of nanoparticles and bulk materials. ACS Catal 2:1765–1772
18. Pei J, Mao J, Liang X, Chen C, Peng Q, Wang D, Li Y (2016) Ir–Cu nanoframes: one-pot synthesis and efficient electrocatalysts for oxygen evolution reaction. Chem comm 52:3793–3796
19. Ji S-M, Muthurasu A, Chhetri K, Kim HY (2022) Metal-organic framework assisted vanadium oxide nanorods as efficient electrode materials for water oxidation. J of Colloid and Interface Sci 618:475–482

20. Sun H, Yan Z, Liu F, Xu W, Cheng F, Chen J (2020) Self-supported transition-metal-based electrocatalysts for hydrogen and oxygen evolution. Adv Mater 32:1806326
21. Anantharaj S, Aravindan V (2020) Developments and perspectives in 3d transition-metal-based electrocatalysts for neutral and near-neutral water electrolysis. Adv Energy Mater 10:1902666
22. She L, Zhao G, Ma T et al (2022) On the durability of iridium-based electrocatalysts toward the oxygen evolution reaction under acid environment. Adv Funct Mater 32:2108465
23. Xu J, Lian Z, Wei B et al (2020) Strong electronic coupling between ultrafine iridium-ruthenium nanoclusters and conductive, acid-stable tellurium nanoparticle support for efficient and durable oxygen evolution in acidic and neutral media. ACS Catal 10:3571–3579
24. Zhang Z, Wang H, Ma M et al (2021) Integrating NiMoO wafer as a heterogeneous 'turbo' for engineering robust Ru-based electrocatalyst for overall water splitting. Chem Eng J 420:127686
25. Lyu F, Wang Q, Choi SM, Yin Y (2019) Noble-metal-free electrocatalysts for oxygen evolution. Small 15:1804201
26. Chhetri K, Tiwari AP, Dahal B, Ojha GP, Mukhiya T, Lee M, Kim T, Chae S-H, Muthurasu A, Kim HY (2020) A ZIF-8-derived nanoporous carbon nanocomposite wrapped with Co3O4-polyaniline as an efficient electrode material for an asymmetric supercapacitor. J of Electroanaly Chem 856:113670
27. Saha S, Ganguli AK (2017) FeCoNi alloy as noble metal-free electrocatalyst for oxygen evolution reaction (OER). ChemSelect 2:1630–1636
28. Gao R, Deng M, Yan Q, Fang Z, Li L, Shen H, Chen Z (2021) Structural variations of metal oxide-based electrocatalysts for oxygen evolution reaction. Small Methods 5:2100834
29. Yu X, He X, Li R, Gou X (2021) One-step synthesis of amorphous nickel iron phosphide hierarchical nanostructures for water electrolysis with superb stability at high current density. Dalton Trans 50:8102–8110
30. Peng LJ, Huang JP, Pan QR, Liang Y, Yin N, Xu HC, Li N (2021) A simple method for the preparation of a nickel selenide and cobalt selenide mixed catalyst to enhance bifunctional oxygen activity for Zn–air batteries. RSC Adv 11:19406–19416
31. Ullah N, Ullah R, Khan S, Xu Y (2021) Boron nitride-based electrocatalysts for HER, OER, and ORR: a mini-review. Front Mater Sci 15:543–552
32. Chhetri K, Dahal B, Mukhiya T, Tiwari AP, Muthurasu A, Kim T, Kim H, Kim HY (2021) Integrated hybrid of graphitic carbon-encapsulated CuxO on multilayered mesoporous carbon f rom copper MOFs and polyaniline for asymmetric supercapacitor and oxygen reduction reactions. Carbon 179:89–99
33. Han N, Luo S, Deng C, Zhu S, Xu Q, Min Y (2021) Defect-rich FeN0. 023/Mo2C heterostructure as a highly efficient bifunctional catalyst for overall water-splitting. ACS appl mater interfaces 13:8306–8314
34. Cui B, Hu Z, Liu C, Liu S, Chen F, Hu S, Zhang J, Zhou W, Deng Y, Qin Z (2021) Heterogeneous lamellar-edged Fe-Ni (OH) 2/Ni3S2 nanoarray for efficient and stable seawater oxidation. Nano Res 14:1149–1155
35. Xu P, Wang H, Liu J, Feng X, Ji W, Au CT (2021) High-performance Ni x Co3-xO4/Ti3C2T x-HT interfacial nanohybrid for electrochemical overall water splitting. ACS Appl Mater Interfaces 13:34308–34319
36. Liu T, Cai S, Zhao G, Gao Z, Liu S, Li H, Chen L, Li M, Yang X, Guo H (2021) Recycling valuable cobalt from spent lithium ion batteries for controllably designing a novel sea-urchin-like cobalt nitride-graphene hybrid catalyst: towards efficient overall water splitting. J Energy Chem 62:440–450
37. Yang F, Xiong T, Huang P, Zhou S, Tan Q, Yang H, Huang Y, Balogun MSJT (2021) Nanostructured transition metal compounds coated 3D porous core-shell carbon fiber as monolith water splitting electrocatalysts: a general strategy. Chem Eng J 423:130279
38. Alsaç EP, Bodappa N, Whittingham AW, Liu Y, de Lazzari A, Smith RD (2021) Structure–property correlations for analysis of heterogeneous electrocatalysts. Chem Phys Rev 2:031306
39. Zhao S, Yang M, Tan Y, Brett DJ, He G, Parkin IP (2021) Facile room-temperature synthesis of cobalt sulphide for efficient oxygen evolution reaction. Multifunct Mater 4:025001
40. Kashinath L (2021) Microwave-hydrothermal synthesis of copper sulphide nanorods embedded on graphene sheets as an efficient electrocatalyst for excellent hydrogen evolution reaction. Fuel 291:120143
41. Ali H, Ghosh S, Mondal A (2021) Nickel sulphide flakes improved cone-shaped graphite electrode for high-performance OER activity. Bull Mater Sci 44:1–9
42. Mane VJ, Kale SB, Ubale SB, Lokhande VC, Patil UM, Lokhande CD (2021) Lanthanum sulfide-manganese sulfide/graphene oxide (La2S3-MnS/GO) composite thin film as an electrocatalyst for oxygen evolution reactions. J Solid State Electrochem 25:1775–1788
43. Nouseen S, Singh P, Lavate S, Chattopadhyay J, Kuchkaev AM, Yakhvarov DG, Srivastava R (2021) Transition metal based ternary hierarchical metal sulphide microspheres as electrocatalyst for splitting of water into hydrogen and oxygen fuel. Catal Today (in press)
44. Wang B, Zhao P, Feng J, Chen D, Huang Y, Sui L, Dong H, Ma S, Dong L, Yu L (2021) Carbon-based 0D/1D/2D assembly with desired structures and defect states as non-metal bifunctional electrocatalyst for zinc-air battery. J Colloid Interface Sci 588:184–195
45. Zhao C-X, Liu J-N, Wang J, Wang C, Guo X, Li X-Y, Chen X, Song L, Li BQ, Zhang Q (2022) A clicking confinement strategy to fabricate transition metal single-atom sites for bifunctional oxygen electrocatalysis. Sci Adv 8:eabn5091
46. Liu B, Wang S, Wang C-Y, Ma B-Z, Chen Y-Q (2020) Electrochemical behavior and corrosion resistance of IrO2-ZrO_2 binary oxide coatings for promoting oxygen evolution in sulfuric acid solution. Int J Miner Metall Mater 27:264–273
47. Li R, Zhang R, Qiao Y, Zhang D, Cui Z, Wang W (2022) Heterostructure Ni (OH) 2/ZrO2 catalyst can achieve efficient oxygen reduction reaction. Chem Eng Sci 250:117398
48. Xie H, Geng Q, Liu X, Mao J (2022) Interface engineering for enhancing electrocatalytic oxygen evolution reaction of CoS/CeO2 heterostructures. Front Chem Sci Eng 16:376–383
49. Yu J, Lu K, Wang C, Wang Z, Fan C, Bai G, Wang G, Yu F (2021) Modification of NiFe layered double hydroxide by lanthanum doping for boosting water splitting. Electrochim Acta 390:138824
50. Sakamaki A, Ogihara H, Yoshida-Hirahara M, Kurokawa H (2021) Precursor accumulation on nanocarbons for the synthesis of $LaCoO_3$ nanoparticles as electrocatalysts for oxygen evolution reaction. RSC Adv 11:20313–20321
51. Wei R, Zhang K, Zhao P, An Y, Tang C, Chen C, Li X, Ma X, Ma Y, Hao X (2021) Defect-rich FeCoNiPB/$(FeCoNi)_3O_{4-x}$ high-entropy composite nanoparticles for oxygen evolution reaction: impact of surface activation. Appl Surface Sci 549:149327
52. Sadaqat M, Nisar L, Hussain F, Ashiq MN, Shah A, Ehsan MF, Najam-Ul-Haq M, Joya KS (2019) Zinc-telluride nanospheres as an efficient water oxidation electrocatalyst displaying a low overpotential for oxygen evolution. J Mater Chem A 7:26410–26420
53. Hu D, Wang X, Yang H, Liu D, Wang Y, Guo J, Wu T (2018) Host-guest electrocatalyst with cage-confined cuprous sulfide nanoparticles in etched chalcogenide semiconductor zeolite for highly efficient oxygen reduction reaction. Electrochimi Acta 282:877–885
54. Zheng YR, Gao MR, Gao Q, Li HH, Xu J, Wu ZY, Yu SH (2015) An efficient CeO2/CoSe2 nanobelt composite for electrochemical water oxidation. Small 11:182–188

55. Galani SM, Mondal A, Srivastava DN, Panda AB (2020) Development of RuO2/CeO2 heterostructure as an efficient OER electrocatalyst for alkaline water splitting. Int J Hydrog Energy 45:18635–18644
56. Swesi AT, Masud J, Nath M (2016) Nickel selenide as a high-efficiency catalyst for oxygen evolution reaction. Energy Environ Sci 9:1771–1782
57. Gozzo CB, Soares MR, Sczancoski JC, Nogueira IC, Leite ER (2019) Investigation of the electrocatalytic performance for oxygen evolution reaction of Fe-doped lanthanum nickelate deposited on pyrolytic graphite sheets. Inter J Hydrog Energy 44:21659–21672
58. Qu M, Jiang Y, Yang M, Liu S, Guo Q, Shen W, Li M, He R (2020) Regulating electron density of NiFe-P nanosheets electrocatalysts by a trifle of Ru for high-efficient overall water splitting. Appl Catal B Environ 263:118324
59. Lu S-S, Zhang L-M, Dong Y-W, Zhang J-Q, Yan X-T, Sun D-F, Shang X, Chi J-Q, Chai Y-M, Dong B (2019) Tungsten-doped Ni–Co phosphides with multiple catalytic sites as efficient electrocatalysts for overall water splitting. J Mater Chem A 7:16859–16866
60. Rodney JD, Deepapriya S, Robinson MC, Raj CJ, Perumal S, Kim BC, Das SJ (2020) Lanthanum doped copper oxide nanoparticles enabled proficient bi-functional electrocatalyst for overall water splitting. Int J Hydrog Energy 45:24684–24696
61. Tian Y, Wang S, Velasco E, Yang Y, Cao L, Zhang L, Li X, Lin Y, Zhang Q, Chen L (2020) A Co-doped nanorod-like RuO2 electrocatalyst with abundant oxygen vacancies for acidic water oxidation. Iscience 23:100756
62. Nazar N, Manzoor S, Rehman Y, Bibi I, Tyagi D, Chughtai AH, Gohar RS, Najam-Ul-Haq M, Imran M, Ashiq MN (2022) Metal-organic framework derived CeO_2/C nanorod arrays directly grown on nickel foam as a highly efficient electrocatalyst for OER. Fuel 307:121823